Journal of Computational Physics 228 (2009) 5101–5110

Contents lists available at ScienceDirect

Journal of Computational Physics

journal homepage: www.elsevier.com/locate/jcp

A class of stable spectral methods for the Cahn–Hilliard equation ☆

Li-ping He [a,*], Yunxian Liu [b]

[a] Department of Mathematics, Shanghai Jiao Tong University, Shanghai 200030, PR China
[b] School of Mathematics, Shandong University, Jinan, Shandong 250100, PR China

ARTICLE INFO

Article history:
Received 16 October 2008
Received in revised form 1 April 2009
Accepted 5 April 2009
Available online 22 April 2009

PACS:
05.10.−a
02.60.Cb
64.75.+g
81.15.Aa

Keywords:
Dissipative spectral method
Cahn–Hilliard model

ABSTRACT

In this work, the initial-boundary value problem of two-dimensional Cahn–Hilliard equation is considered. A class of fully discrete dissipative Fourier spectral schemes are proposed. Moreover, semi-implicit prediction–correction schemes are presented. The numerical simulations are performed to demonstrate the effectiveness of the proposed schemes.

© 2009 Elsevier Inc. All rights reserved.

1. Introduction

In this paper, the Fourier spectral approximations of the Cahn–Hilliard model

$$\begin{cases} \partial_t u + M\Delta(\gamma\Delta u - \phi(u)) = 0, & (x,y) \in \Omega, \quad t > 0, \\ u(x,y,0) = u_0(x,y), & (x,y) \in \Omega, \end{cases} \tag{1}$$

with periodic boundary conditions on the square $\Omega = (0, 2\pi)^2$ are presented, where M is the mobility constant, $\gamma > 0$ is a phenomenological constant modelling the effect of interfacial energy, u is the order parameter,

$$w = \phi(u) - \gamma\Delta u$$

is a generalized chemical potential energy with $\phi(u) = \psi\prime(u)$. Here,

$$\psi(u) = \frac{1}{4}(u^2 - 1)^2$$

is an approximation of the free energy corresponding to the binodal points $u = +1$ and $u = -1$ and spinodal interval $(-1/\sqrt{3}, 1/\sqrt{3})$. Without lose of generality, we assume $M = 1$. Define

$$\mathcal{F}(u) = \int_\Omega \left(\psi(u) + \frac{\gamma}{2}|\nabla u|^2\right) d\Omega.$$

☆ The research of the author is supported in part by NNSF of China grant 10501031.
* Corresponding author. Tel.: +80 21 64640589.
E-mail addresses: lphe@sjtu.edu.cn, lphe@ann.jussieu.fr (L.-p. He).

0021-9991/$ - see front matter © 2009 Elsevier Inc. All rights reserved.
doi:10.1016/j.jcp.2009.04.011

Then it can be verified that

$$\frac{\mathrm{d}}{\mathrm{d}t}\mathcal{F}(u)+\int_{\Omega}|\nabla w|^2\mathrm{d}\Omega=0, \tag{2}$$

which yields

$$\frac{\mathrm{d}}{\mathrm{d}t}\mathcal{F}(u)\leqslant 0. \tag{3}$$

Hence, the total energy $\mathcal{F}(u)$, the sum of the free energy $\int_{\Omega}\psi(u)\mathrm{d}\Omega$ and the interfacial energy $\int_{\Omega}\frac{\gamma}{2}|\nabla u|^2\mathrm{d}\Omega$, is dissipative. This means that the phase separation evolution is from a higher initial state into a lower energy state. Also, the mass conservation holds as follows:

$$\frac{1}{|\Omega|}\int_{\Omega}u(x,y,t)\mathrm{d}\Omega=\frac{1}{|\Omega|}\int_{\Omega}u_0(x,y)\mathrm{d}\Omega,\quad t>0. \tag{4}$$

The Cahn–Hilliard model was originally introduced in [3] to describe the phase separation phenomena. There has been a significant research interest in this model (see, e.g., [4,7,12,16,19–21,27]) and the references therein. Several finite element schemes were studied with mathematical rigor by Barrett et al. [1] and Elliott et al. [8–11]. Recently, Feng and Prohl [14] proposed the finite element method for a class of Cahn–Hilliard equation involving a small parameter. Error estimates with quasi-optimal order in time and optimal order in space are obtained for their proposed methods under minimum regularity assumptions on the initial data and the domain. With finite difference approaches, Sun [22] proposed a linearized second-order finite difference scheme which is uniquely solvable in a discrete $L^2(\Omega)$-norm. In Furihata [15], a conservative finite difference scheme was proposed to solve the one-dimensional Cahn–Hilliard equation. It is proved that their scheme is stable in the sense that the decay of energy is preserved. In [18,26], a combined spectral and large time-stepping methods were proposed and studied for the nonlinear diffusion equations for thin film epitaxy. In He and Liu [19], the convergence of the spatial discretization of the Cahn–Hilliard is considered. In resent study [5,13,23], the unconditionally stable algorithms were developed for Cahn–Hillard equation. These algorithms allow for an increasing time step in Cahn–Hillard systems as time proceeds.

The purpose of this paper is to investigate new dissipative numerical schemes for the Cahn–Hilliard equation based on the alternative strategy. In Section 2, we propose a class of the fully discrete dissipative spectral schemes and establish the discrete analogues of (2)–(4). In Section 3, the accuracy tests are carried out. The final section is devoted to the numerical simulations for the temporal evolution of the morphological patterns during a spinodal decomposition and subsequent coarsening. The numerical results using the proposed schemes are presented to demonstrate the effectiveness of our schemes.

2. Dissipative spectral approximation

Let $C_p^{\infty}(\Omega)$ be the sets of all restrictions onto Ω of all 2π-periodic, C^{∞}-functions on R^2. For any $r\geqslant 0$ let $H_p^r(\Omega)$ be the closure of $C_p^{\infty}(\Omega)$ in the usual Sobolev norm of $H^r(\Omega)$. The inner product, the semi-norm and the norm of Sobolev space $H_p^r(\Omega), r\geqslant 0$ are defined by

$$(u,v)_r=\sum_{m,n=-\infty}^{+\infty}(1+m^2+n^2)^r\hat{u}_{m,n}\bar{\hat{v}}_{m,n},\quad |u|_r=\left(\sum_{m,n=-\infty}^{+\infty}(m^2+n^2)^r|\hat{u}_{m,n}|^2\right)^{\frac{1}{2}}$$

and $\|u\|_r=\sqrt{(u,u)_r}$, respectively. If $r=0$, then the index r is omitted. Clearly, $\|\nabla u\|=|u|_1, \|\Delta u\|=|u|_2$, etc. For simplicity, denote $L^2(\Omega)=H_p^0(\Omega)$. Further let $H_p^{-r}(\Omega)$ be the dual space of $H_p^r(\Omega)$, and $\langle u,v\rangle_{L(H_p^{-r},H_p^r)}$ be the duality paring between $H_p^{-r}(\Omega)$ and $H_p^r(\Omega)$. Let $\partial_t u=\frac{\partial u}{\partial t}$, etc.

2.1. Dissipative spectral schemes

For given function $u_0\in L^2(\Omega)$, the weak solution of (1) is a function $u\in L^{\infty}(0,T;L^2(\Omega))\cap L^2(0,T;H_p^2(\Omega))$ such that

$$\begin{cases}(\partial_t u,v)+\gamma(\Delta u,\Delta v)-(\phi(u),\Delta v)=0,\quad \forall v\in H_p^2(\Omega),\quad t\in(0,T],\\ u(x,y,0)=u_0(x,y).\end{cases} \tag{5}$$

Since Fourier spectral method is one of the most suitable spatial approximation methods for periodic problems [2,6,25], it will be employed to handle the spatial discretization. Denote

$$S_N=\mathrm{span}\{e^{i(mx+ny)}|-N\leqslant m,\ n\leqslant N-1\}.$$

Moreover, we define the orthogonal projection operator $P_N: L^2(\Omega)\to S_N$ such that

$$(u - P_N u, v) = 0, \quad \forall v \in S_N.$$

Our main interest in this work is to investigate the time-stepping methods for the problem (1). Let τ be the time step. Set $u^k(x,y) = u(x,y,k\tau)$, also denoted by u^k for simplicity. Let $u_N^k \in S_N$ be the approximation to the solution of (1) at time $t_k = k\tau$. Denote the nonlinear term $\phi(u) = u(u^2 - 1)$. The classical first-order semi-implicit scheme (BD1) in [4] reads as follows

$$\begin{cases} \frac{1}{\tau}(u_N^{k+1} - u_N^k) + \gamma\Delta^2 u_N^{k+1} = P_N\Delta\phi(u_N^k), \\ u_N^0 = P_N u_0(x,y). \end{cases}$$

In practice, it is known that the semi-implicit treatment in time allows a consistently large time step size. Their numerical simulations indicate that the time step in a semi-implicit method can be two orders of magnitude larger than that in an explicit method. The accuracy in time can be improved by using higher-order semi-implicit schemes. For instance, a second-order backward differentiation for $\partial_t u$ and a second-order Adams–Bashforth for the explicit treatment of the nonlinear term for (1) lead to the following second-order scheme (BD2/AB)

$$\begin{cases} \frac{1}{2\tau}(3u_N^{k+1} - 4u_N^k + u_N^{k-1}) + \gamma\Delta^2 u_N^{k+1} = P_N\Delta(2\phi(u_N^k) - \phi(u_N^{k-1})), \\ u_N^0 = P_N u_0(x,y). \end{cases}$$

Also, we can use the second-order semi-implicit Runge–Kutta scheme (SIRK2) in [17], which gives the following time discretization scheme

$$\begin{cases} \frac{1}{\tau}\left(u_{N,\mathrm{pre}}^{k+1} - u_N^k\right) + \frac{\gamma}{2}\Delta^2\left(u_{N,\mathrm{pre}}^{k+1} + u_N^k\right) = P_N\Delta\phi(u_N^k), \\ \frac{1}{\tau}(u_N^{k+1} - u_N^k) + \frac{\gamma}{2}\Delta^2(u_N^{k+1} + u_N^k) = \frac{1}{2}P_N\Delta\left(\phi\left(u_{N,\mathrm{pre}}^{k+1}\right) + \phi(u_N^k)\right), \\ u_N^0 = P_N u_0(x,y). \end{cases}$$

However, these schemes are not dissipative. We now describe our new time-stepping method. Denote

$$\Phi_0(u,v,\alpha) = \left(\frac{u+v}{2}\right)(\alpha u^2 + (1-\alpha)v^2 - 1).$$

Clearly, $\Phi_0(u,u,\alpha) = \phi(u)$. In particular,

$$\Phi_0\left(u_N^{k+1}, u_N^k, \frac{1}{2}\right) = \left(\frac{u_N^{k+1} + u_N^k}{2}\right)\left(\frac{(u_N^{k+1})^2 + (u_N^k)^2}{2} - 1\right).$$

Hence, we can use $\Phi_0(u_N^{k+1}, u_N^k, \alpha)$ to approximate the nonlinear term $\phi(u^k)$, which is different from the Runge–Kutta method. The fully discrete spectral scheme for solving (1) is as follows:

$$\begin{cases} \frac{1}{\tau}(u_N^{k+1} - u_N^k) + \frac{\gamma}{2}\Delta^2(u_N^{k+1} + u_N^k) - P_N\Delta\Phi_0(u_N^{k+1}, u_N^k, \alpha) = 0, \quad k \geqslant 1, \\ u_N^0 = P_N u_0(x,y). \end{cases} \tag{6}$$

Moreover, we use the large time-stepping method in [26] and propose the following scheme

$$\begin{cases} \frac{1}{\tau}(u_N^{k+1} - u_N^k, v) + \beta\tau(\nabla(u_N^{k+1} - u_N^k), \nabla v) + \frac{\gamma}{2}(\Delta(u_N^{k+1} + u_N^k), \Delta v) \\ \qquad\qquad -(\Phi_0(u_N^{k+1}, u_N^k, \alpha), \Delta v) = 0, \quad \forall v \in S_N, \quad k \geqslant 1, \\ u_N^0 = P_N u_0(x,y). \end{cases} \tag{7}$$

It is observed that scheme (7) becomes scheme (6) if $\beta = 0$. Let

$$\Phi(u,v,\alpha) = \Phi_0(u,v,\alpha) + \beta\tau(u - v), \quad \forall u, v \in S_N.$$

An alternative formulation of (7) is to find $u_N^{k+1} \in S_N$ satisfying

$$\begin{cases} \frac{1}{\tau}(u_N^{k+1} - u_N^k) + \frac{\gamma}{2}\Delta^2(u_N^{k+1} + u_N^k) - P_N\Delta\Phi(u_N^{k+1}, u_N^k, \alpha) = 0, \quad k \geqslant 1, \\ u_N^0 = P_N u_0(x,y). \end{cases} \tag{8}$$

We now turn to establish the discrete analogues of (2)–(4). Let $\alpha \geqslant \frac{1}{2}$ and $\beta \geqslant 0$. If u_N^k is the numerical solution of scheme (7), then the total energy is dissipative:

$$\mathcal{F}(u_N^{k+1}) \leqslant \mathcal{F}(u_N^k), \quad k \geqslant 0. \tag{9}$$

In fact, it is easy to be show that

$$\mathcal{F}(u_N^{k+1}) - \mathcal{F}(u_N^k) = -\left(\alpha - \frac{1}{2}\right)\frac{1}{2\tau}\int_\Omega \left((u_N^{k+1})^2 - (u_N^k)^2\right)^2 \mathrm{d}\Omega - \beta\int_\Omega (u_N^{k+1} - u_N^k)^2 \mathrm{d}\Omega$$
$$- \tau\int_\Omega \left|\nabla\left(P_N\Phi(u_N^{k+1}, u_N^k, \alpha) - \frac{\gamma}{2}\Delta(u_N^{k+1} + u_N^k)\right)\right|^2 \mathrm{d}\Omega.$$

By taking $v = 1$ in (7), we find that

$$\int_\Omega u_N^{k+1}(x,y)\mathrm{d}\Omega = \int_\Omega u_N^k(x,y)\mathrm{d}\Omega = \int_\Omega P_N u_0(x,y)\mathrm{d}\Omega, \tag{10}$$

which implies the mass conservation.

From (9), we see that

$$\int_\Omega \left(\psi(u_N^k) + \frac{\gamma}{2}|\nabla u_N^k|^2\right)\mathrm{d}\Omega = \mathcal{F}(u_N^k) \leqslant \mathcal{F}(u_N^0).$$

On the other hand, by using the Poincaré inequality, we obtain from (10) that

$$\left\|u_N^k - \frac{1}{|\Omega|}\int_\Omega P_N u_0(x,y)\mathrm{d}\Omega\right\| = \left\|u_N^k - \frac{1}{|\Omega|}\int_\Omega u_N^k(x,y)\mathrm{d}\Omega\right\| \leqslant \|\nabla u_N^k\|.$$

Hence, if $u_0(x,y) \in H_p^1(\Omega)$, $\alpha \geqslant \frac{1}{2}$ and $\beta \geqslant 0$, we have the a priori estimation as follows:

$$|||u_N|||_{L^\infty(0,T;H_p^1(\Omega))} = \max_k \|u_N^k\|_1 \leqslant C(\Omega, \|u_0\|_1, \gamma).$$

Thus the scheme (7) is stable.

2.2. The semi-implicit schemes

Let $\alpha \geqslant \frac{1}{2}$ and $\beta \geqslant 0$. Given an integer $m \geqslant 1$, the implementation of the dissipative implicit scheme (7) is to find $u_N^{k+1} \in S_N$ satisfying

$$\begin{cases} \frac{1}{\tau}\left(u_N^{k+1,[0]} - u_N^k\right) + \frac{\gamma}{2}\Delta^2\left(u_N^{k+1,[0]} + u_N^k\right) - \beta\tau\Delta\left(u_N^{k+1,[0]} - u_N^k\right) = P_N\Delta\phi(u_N^k), \\ \frac{1}{\tau}\left(u_N^{k+1,[m]} - u_N^k\right) + \frac{\gamma}{2}\Delta^2\left(u_N^{k+1,[m]} + u_N^k\right) - \beta\tau\Delta\left(u_N^{k+1,[m]} - u_N^k\right) = P_N\Delta\Phi_0\left(u_N^{k+1,[m-1]}, u_N^k, \alpha\right), \\ u_N^{k+1} = u^{k+1,[m]}, \quad m = 1,2,\ldots, \quad k \geqslant 1, \\ u_N^0 = P_N u_0(x,y). \end{cases} \tag{11}$$

In particular, in the case of $m = 1$, we obtain the semi-implicit prediction–correction scheme as follows:

$$\begin{cases} \frac{1}{\tau}\left(u_{N,\mathrm{pre}}^{k+1} - u_N^k\right) + \frac{\gamma}{2}\Delta^2\left(u_{N,\mathrm{pre}}^{k+1} + u_N^k\right) - \beta\tau\Delta\left(u_{N,\mathrm{pre}}^{k+1} - u_N^k\right) = P_N\Delta\phi(u_N^k), \\ \frac{1}{\tau}(u_N^{k+1} - u_N^k) + \frac{\gamma}{2}\Delta^2(u_N^{k+1} + u_N^k) - \beta\tau\Delta(u_N^{k+1} - u_N^k) = P_N\Delta\Phi_0\left(u_{N,\mathrm{pre}}^{k+1}, u_N^k, \alpha\right), \\ u_N^0 = P_N u_0(x,y). \end{cases} \tag{12}$$

The existence and uniqueness of (11) and (12) are easy to show by using the Lax–Milgram theorem. In the Fourier space, (12) can be written as

$$\begin{cases} \tilde{u}_{\mathrm{pre}}^{k+1}(\mathbf{k}) = A(\mathbf{k})\tilde{u}^k(\mathbf{k}) - B(\mathbf{k})\left\{\tilde{\phi}(u_N^k)\right\}_{\mathbf{k}}, \\ \tilde{u}^{k+1}(\mathbf{k}) = A(\mathbf{k})\tilde{u}^k(\mathbf{k}) - B(\mathbf{k})\left\{\tilde{\Phi}_0\left(u_{N,\mathrm{pre}}^{k+1}, u_N^k, \alpha\right)\right\}_{\mathbf{k}}, \end{cases}$$

where $\mathbf{k} = (k_1, k_2)$ is a vector in the Fourier space, $-\frac{N}{2} \leqslant k_1, k_2 \leqslant \frac{N}{2} - 1$, $|\mathbf{k}| = \sqrt{k_1^2 + k_2^2}$ is the magnitude of $\mathbf{k}$, $\tilde{u}^k(\mathbf{k})$ and $\left\{\tilde{\phi}(u_N^k)\right\}_{\mathbf{k}}$ represent the Fourier transforms of u_N^k and $\phi(u_N^k)$, respectively;

$$A(\mathbf{k}) = \left(1 + \tfrac{1}{2}\gamma\tau|\mathbf{k}|^4 + \beta\tau^2|\mathbf{k}|^2\right)^{-1}\left(1 - \tfrac{1}{2}\gamma\tau|\mathbf{k}|^4 + \beta\tau^2|\mathbf{k}|^2\right),$$
$$B(\mathbf{k}) = \left(1 + \tfrac{1}{2}\gamma\tau|\mathbf{k}|^4 + \beta\tau^2|\mathbf{k}|^2\right)^{-1}\tau|\mathbf{k}|^2.$$

We now describe the algorithm of (11) by an offline–online procedure.

Offline Stage

In the offline stage, all of the following precomputing are performed only once.

1. Calculate $\tilde{u}^0(\mathbf{k})$ and $\left\{\tilde{\phi}(u_N^0)\right\}_{\mathbf{k}}$.
2. Evaluate and store $A(\mathbf{k})$ and $B(\mathbf{k})$.

Online Stage

In the online stage we share the advantage of the explicit scheme. So we need only compute

$$\begin{cases} \tilde{u}^{k+1,[0]}(\mathbf{k}) = A(\mathbf{k})\tilde{u}^{k}(\mathbf{k}) - B(\mathbf{k})\left\{\tilde{\phi}\left(u_N^k\right)\right\}_{\mathbf{k}}, \\ \tilde{u}^{k+1,[n]}(\mathbf{k}) = A(\mathbf{k})\tilde{u}^{k}(\mathbf{k}) - B(\mathbf{k})\left\{\tilde{\Phi}_0\left(u_N^{k+1,[n-1]}, u_N^k, \alpha\right)\right\}_{\mathbf{k}}, \quad n = 1,2,\ldots,m \end{cases}$$

in which $\tilde{u}^k(\mathbf{k}) = \tilde{u}^{k,[m]}(\mathbf{k})$ for $k \geqslant 1$. To reduced the computational cost, the nonlinear term should be evaluated by using the Orszag's transform method.

We list two important results as follows.

- (a) If $\alpha = \frac{1}{2}$, by using the method in [17] we can show that the scheme (12) is second-order in time for any τ.
- (b) If $\alpha = 1$, the scheme (12) is first-order in time.

3. Accuracy test

We now consider the accuracy test. To this end, we define the relative error as

$$E^*(u(t)) = \frac{\|u(t) - u_N(t)\|_{L^\infty(\Omega)}}{\|u(t)\|_{L^\infty(\Omega)}}.$$

Since the exact solution for problem (1) is unknown, we use numerical results of the scheme (12) with $\tau_e = 0.01\tau$ and $N_e = N$ as the "exact" solution.

In this section, we consider (1) with the initial value

$$u(x,y,0) = \sin\left(\frac{2\pi}{L}x\right)\sin\left(\frac{2\pi}{L}y\right),$$

where L is the periodic in space x and y. In all calculations, we take $L = 10, T = 1$, $\gamma = 0.2$ and $N = 128$.

The numerical results are presented in Tables 1 and 2. Table 1 shows that scheme (11) is second-order accurate in time if $\alpha = \frac{1}{2} + O(\tau)$. Table 2 indicates that the scheme (12) is of second-order in time for any τ if $\alpha = \frac{1}{2}$. Several other values of α are also considered in the case $\beta \neq 0$.

We now carry out numerical simulations using the scheme (12). A $N \times N$ Fourier modes has been used on the square $[0,N] \times [0,N]$. The morphological evolution from the "as-quenched" state of the system which is determined by an initial condition $u(x,y,0) = u_0 + \delta u(x,y)$, where u_0 is the average composition of the solution and $\delta u(x,y)$ is a random perturbation with values distributed uniformly between $+0.05$ and -0.05. Hence, we have to control the numerical errors. We point out here that the small perturbations are generated by a random number generator. In all calculations, we take $u_0 = -0.45$, $\gamma = 0.5$ and the same initial value for the same N.

The numerical results are presented in Tables 3–5. In Table 3, we compare the scheme (12) in the case $\alpha = 1$ (PC1), which is a first-order scheme, with the scheme BD1. It indicates that PC1 is better than BD1. Also, we discusses the choice of β for $\alpha = 1$.

Table 4 compares the prediction–correction scheme (12) in the case $\alpha = 0.5$ and $\beta = 0$ (PC2) with other second-order schemes. It indicates that PC2 is better than SIRK2 and BD2/AB. In Table 5, we consider the errors of scheme (11) with $\alpha = 0.5$ and $\beta = 0$ for different iterative number m. It shows that PC2 provides very accurate numerical results.

4. Numerical simulations

In this section some results of the simulations using the scheme (12) with $N = 128, \alpha = 0.5$ and $m = 1$ are shown. The time step τ is chosen to be 0.5 although as large as 2 can be used (see Fig. 6). A 128×128 Fourier modes has been used on the square $[0,128] \times [0,128]$. The morphological evolution from the "as-quenched" state of the system which is determined by an initial condition $u(x,y,0) = u_0 + \delta u(x,y)$, where u_0 is the average composition of the solution and $\delta u(x,y)$ is a random perturbation with values distributed uniformly between $+0.05$ and -0.05. Typical spatial and temporal evolutions

Table 1
The error $E^*(u(1))$ obtained by using scheme (11) with $\beta = 0$.

α	$m = 1$			$m = 2$		
	$\tau = 0.1$	$\tau = 0.01$	$\tau = 0.001$	$\tau = 0.1$	$\tau = 0.01$	$\tau = 0.001$
0.51	7.3E−4	2.7E−5	1.5E−6	4.0E−4	1.1E−5	1.3E−6
0.52	8.6E−4	4.1E−5	2.8E−6	4.6E−4	2.4E−5	2.6E−6
0.53	1.0E−3	5.4E−5	4.1E−6	5.2E−4	3.7E−5	3.9E−6
0.54	1.1E−3	6.8E−5	5.5E−6	5.8E−4	5.1E−5	5.3E−6
0.55	1.3E−3	8.2E−5	6.8E−6	6.4E−4	6.4E−5	6.6E−6

Table 2
The error $E^*(u(1))$ obtained by using scheme (11) with $m = 1$.

α	$\beta = 0$			$\beta = 0.001$		
	$\tau = 0.1$	$\tau = 0.01$	$\tau = 0.001$	$\tau = 0.1$	$\tau = 0.01$	$\tau = 0.001$
0.5	6.0E−4	1.5E−5	2.0E−7	6.0E−4	1.5E−5	2.0E−7
0.75	4.5E−3	3.5E−4	3.3E−5	4.5E−3	3.5E−4	3.3E−5
1	9.7E−3	7.0E−4	6.7E−5	9.7E−3	7.0E−4	6.7E−5

Table 3
The error $E^*(u(10))$ obtained by using scheme (12) with $\alpha = 1$ and $m = 1$.

N	BD1		PC1		$\beta = 0.25$		$\beta = 0.5$		$\beta = 1$	
	$\tau = 0.1$	$\tau = 0.01$	$\tau = 0.1$	$\tau = 0.01$	$\tau = 0.1$	$\tau = 0.01$	$\tau = 0.1$	$\tau = 0.01$	$\tau = 0.1$	$\tau = 0.01$
64	1.5E−3	1.5E−4	7.0E−4	7.1E−5	8.1E−4	7.2E−5	9.1E−4	7.3E−5	1.1E−3	7.5E−5
128	1.7E−3	1.7E−4	7.9E−4	7.9E−5	8.1E−4	8.0E−5	9.1E−4	8.1E−5	1.0E−3	8.3E−5
256	2.3E−3	2.3E−4	8.9E−4	8.8E−5	8.3E−4	9.1E−5	9.2E−4	9.1E−5	1.3E−3	9.2E−5

Table 4
The error $E^*(u(10))$ using different temporal discretization schemes.

N	SIRK2		BD2/AB		PC2	
	$\tau = 0.1$	$\tau = 0.01$	$\tau = 0.1$	$\tau = 0.01$	$\tau = 0.1$	$\tau = 0.01$
64	1.3E−4	1.5E−6	6.9E−5	3.4E−6	4.9E−5	5.9E−7
128	1.4E−4	1.6E−6	9.4E−5	4.5E−6	4.8E−5	6.1E−7
256	1.2E−4	1.4E−6	1.1E−4	4.4E−6	5.2E−5	6.3E−7

Table 5
The error $E^*(u(t)), \alpha = 0.5, \beta = 0, \tau = 0.1$.

t	PC2			$m = 2$		
	$N = 64$	$N = 128$	$N = 256$	$N = 64$	$N = 128$	$N = 256$
2	1.3E−4	1.6E−4	1.6E−4	1.4E−4	1.7E−4	1.8E−4
4	4.6E−5	4.6E−5	4.4E−5	4.2E−5	5.0E−5	4.3E−5
6	4.5E−5	4.4E−5	4.1E−5	4.2E−5	4.7E−5	3.9E−5
8	4.6E−5	4.5E−5	4.1E−5	4.4E−5	4.8E−5	4.1E−5
10	4.9E−5	4.8E−5	5.2E−5	4.7E−5	5.1E−5	4.5E−5

of the "as-quenched" microstructures are presented in Figs. 1–5 for $u_0 = 0$ and 0.45, respectively, in the spinodal region. The simulations show that initial compositions which are perturbations of a uniform state in the spinodal interval evolve rapid into a phase separated structure. After this rapid evolution a slow coarsening process takes place involving an increase of the size of the phase domains.

In Figs. 1–3, we presented the temporal evolution of morphological patterns during spinodal decomposition and subsequent coarsening without the elastic strain effect; and thus we improve the corresponding results in Copetti and Elliot [7].

In Wang et al. [24], a microscopic kinetic model including the elastic strain effect were considered to simulate the morphological evolution controlled by a transformation-induced elastic strain during a solid state precipitation. Chen and Shen [4] considered the Cahn–Hillard model in the case $u_0 = 0$. We now consider the microstructure evolution in elastically homogeneous coherent two-phase solids using the Cahn–Hilliard equation. In coherent systems, one of the main contributions to the total driving force for microstructure evolution is the elastic strain energy caused by the lattice mismatch between the two phase. It is safe to assume that the mechanical equilibrium in a system is established much faster than any diffusion processes. As a result, the system is always at mechanical equilibrium during phase separation or during coarsening. Therefore, at each time step, the mechanical equilibrium equations have to be solved either numerically or analytically. It was shown by Khachaturyan that, in the homogeneous modulus approximation, the elastic energy of any arbitrary microstructure can be analytically calculated. However, the elastic energy is a double-volume integral of infinitely long-ranged elastic interactions in real space, and its contribution to the total driving force enters the Eq. (1) as a volume integral, a nonlocal term (see [4,24]). Therefore, direct numerical solution in real space is prohibitively difficult. In Fourier space, the elastic energy is reduced to a single volume integral of the Fourier transform of the elastic interactions. For example, for the scheme (12), we need only modify $A(\mathbf{k})$ and $B(\mathbf{k})$ on the offline stage as

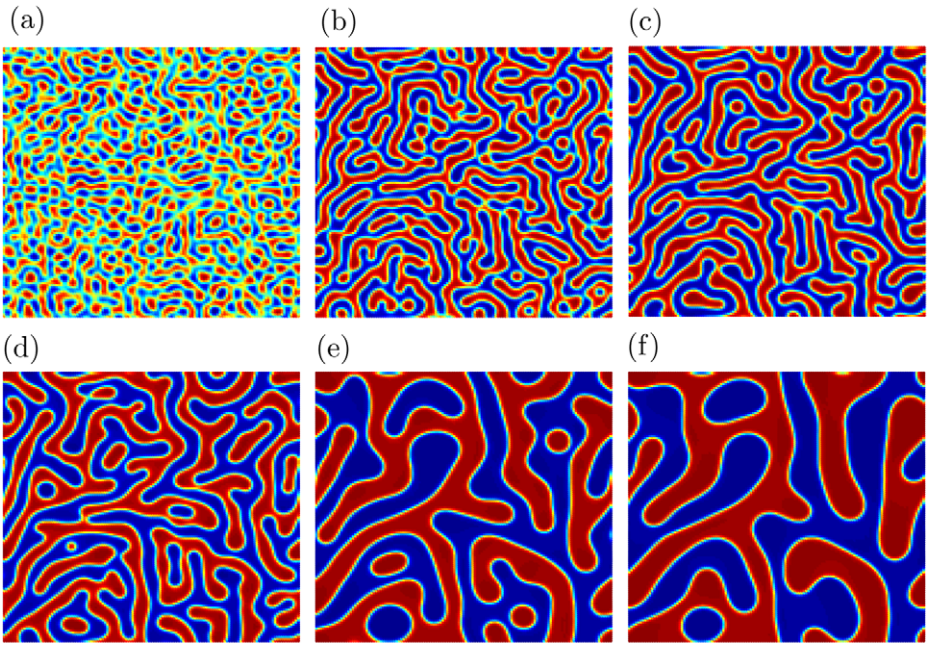

Fig. 1. Temporal morphological evolutions with $\gamma = 0.5$ and $u_0 = 0$ at different time: (a) $t = 10$; (b) $t = 30$; (c) $t = 50$; (d) $t = 100$; (e) $t = 500$; (f) $t = 1000$.

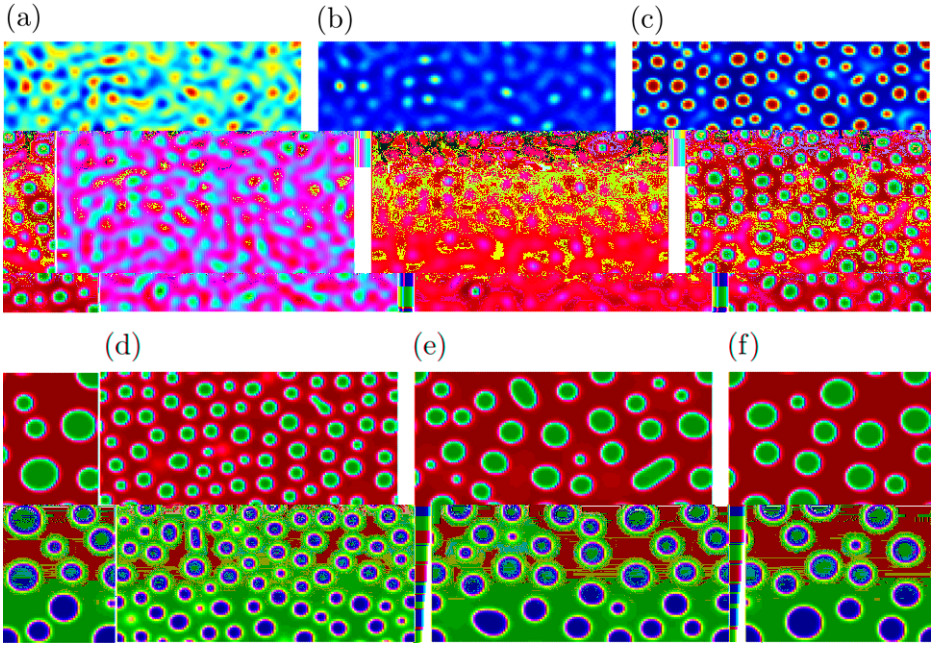

Fig. 2. Same as Fig. 1, except with $u_0 = 0.45$.

$$A(\mathbf{k}) = \left(1 + \frac{1}{2}\tau B(e)|\mathbf{k}|^2 + \frac{1}{2}\gamma\tau|\mathbf{k}|^4 + \beta\tau^2|\mathbf{k}|^2\right)^{-1}\left(1 - \frac{1}{2}\tau B(e)|\mathbf{k}|^2 - \frac{1}{2}\gamma\tau|\mathbf{k}|^4 + \beta\tau^2|\mathbf{k}|^2\right),$$
$$B(\mathbf{k}) = \left(1 + \frac{1}{2}\tau B(e)|\mathbf{k}|^2 + \frac{1}{2}\gamma\tau|\mathbf{k}|^4 + \beta\tau^2|\mathbf{k}|^2\right)^{-1}\tau|\mathbf{k}|^2. \tag{13}$$

where e is a unit vector in Fourier space and $B(e)$ is the Fourier transform of the long-range elastic interactions. For a cubic two-phase solid and assuming that the lattice parameter difference between the two phase is directly proportional to their compositional difference, i.e., Vegard's law, in a two-dimensional model, $B(e)$ is given by [4,24]

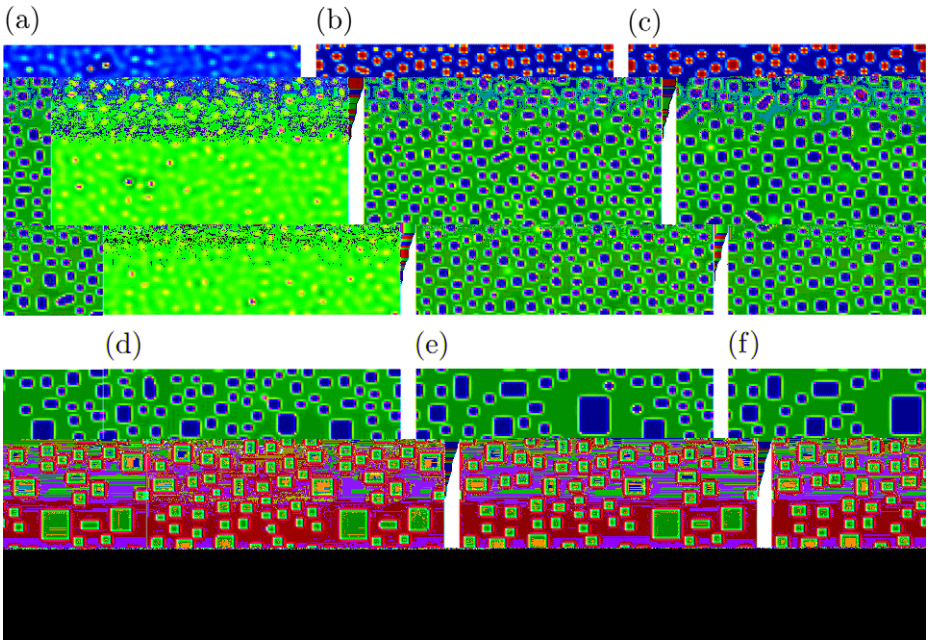

Fig. 3. The morphological evolutions with $\gamma = 0.2$ and $u_0 = 0.45$ at different time: (a) $t = 10$; (b) $t = 50$; (c) $t = 100$; (d) $t = 1000$; (e) $t = 2000$; (f) $t = 3000$.

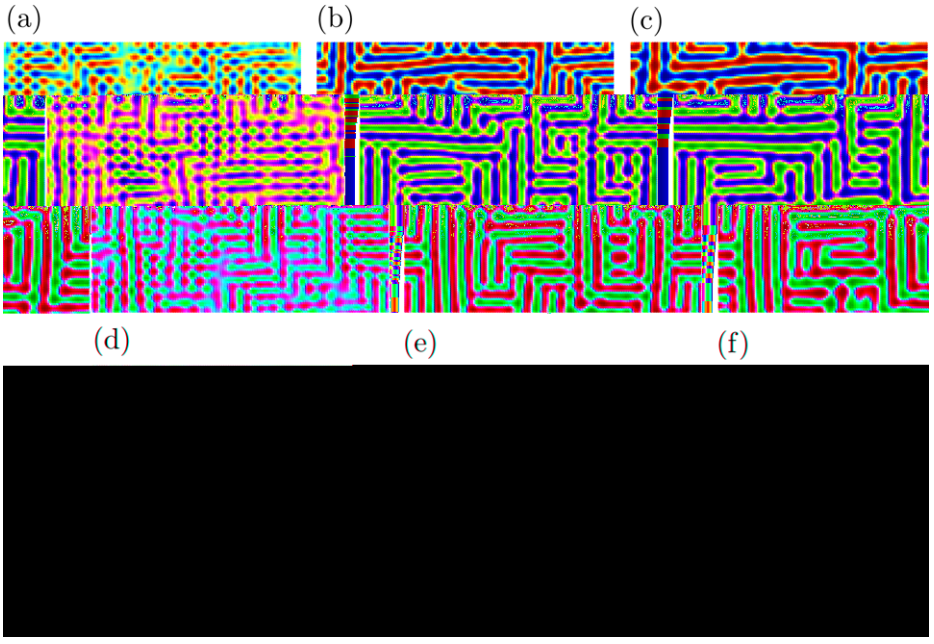

Fig. 4. The morphological evolutions with $\gamma = 0.5, u_0 = 0$ and $B_{el} = 2$ at different time: (a) $t = 10$; (b) $t = 30$; (c) $t = 50$; (d) $t = 100$; (e) $t = 500$; (f) $t = 1000$.

$$B(e) \cong B_{el} e_x^2 e_y^2,$$

where e_x and e_y are the x and y components of the unit vector e, and $B(e)$ is a material constant which depends on the elastic constants and misfit strain. A positive value for B_{el} represents a system with negative elastic anisotropy. It is clear from (13) that the elastic energy contribution to the total driving force have no more cost on the online stage. In Figs. 4 and 5, we pre-

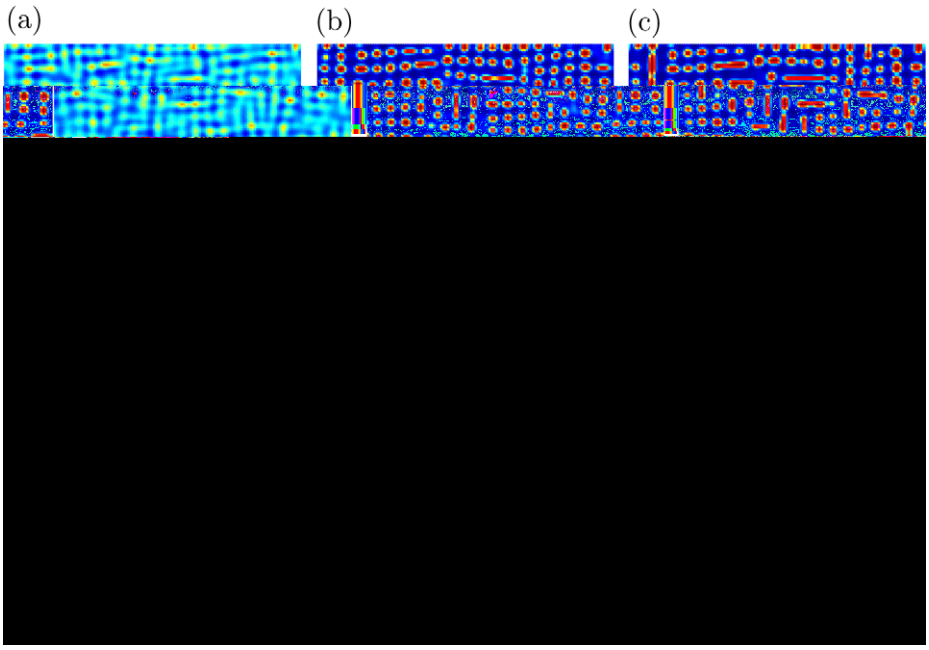

Fig. 5. The morphological evolutions with $\gamma = 0.2, u_0 = 0.45$ and $B_{el} = 1.25$ at different time: (a) $t = 10$; (b) $t = 30$; (c) $t = 50$; (d) $t = 100$; (e) $t = 500$; (f) $t = 1000$.

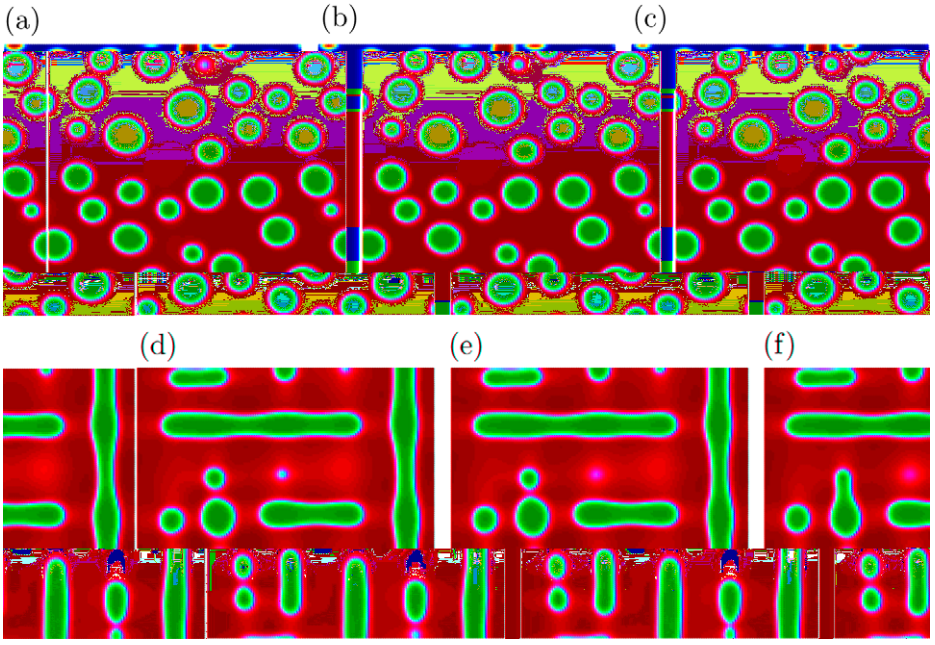

Fig. 6. The morphological evolutions at time $t = 1000$ for different time step, $\gamma = 1, u_0 = 0.45$: (a) $B_{el} = 0$, $\tau = 0.5$; (b) $B_{el} = 0$, $\tau = 1$; (c) $B_{el} = 0$, $\tau = 2$; (d) $B_{el} = 1$, $\tau = 0.5$; (e) $B_{el} = 1$, $\tau = 1$; (f) $B_{el} = 1$, $\tau = 2$.

sented the temporal evolution of strain-dominated morphological patterns during spinodal decomposition and subsequent coarsening.

We point out here, our implicit time discretization for the elastic energy is different from the explicit discretization in [4,24], and thus the scheme is still stable. In Fig. 6, we present the simulation results for different time step. A fixed algorithmic time step driving scheme may also provide significant speedup.

5. Conclusions

In this paper, we have presented a class of stable spectral schemes for the Cahn–Hillard equation. We have demonstrated that a fixed algorithmic time step driving scheme may provide higher accuracy and significant speedup. Although our algorithms allow large algorithmic time steps, caution is indicated, as taking too large an algorithmic time step will yield inaccuracies. This saturation in the speedup results from the details of how the system's energy evolution (and its corresponding microstructural evolution) is governed by the effective time step.

Although we have only considered the periodic boundary conditions here, the dissipative schemes can also be efficiently applied to the time-dependent Ginzburg–Landau (TDGL) and Cahn–Hilliard equations with Dirichlet, Neumann or mixed boundary conditions by using the Legender spectral or spectral element methods. On the other hand, the proposed method has also its limitations. It is most efficient when applied to problems whose principal elliptic operators have constant coefficients, although problems with variable coefficients can be treated with slightly less efficiency, for instance, by an iterative procedure or by a collocation approach. Also, since the proposed method uses a uniform grid for the spatial variables, it may have difficult to resolve extremely sharp interfaces with a moderate number of grid points. In this case, an adaptive spectral method may become more appropriate.

It is expected that the numerical schemes proposed in this work may have extensive applications in a wide class of non-equilibrium systems. For example, it can be applied to the phase field crystal model and martensitic transformations. This method should allow researchers to dramatically improve the computational efficiency and accuracy associated with modeling the dynamics of materials systems. On the other hand, the present methodology developed in this paper is certainly limited to the dynamical model of transport that only has a first-order of time derivative of the order parameter. It would certainly be interesting to attempt to extend this methodology to the dynamics of phase transitions that contain higher-order term, such as those that violate the assumption of local equilibrium. Theoretical analysis for the dissipative schemes also seems challenging.

References

[1] J.W. Barrett, J.F. Blowey, H. Garcke, On fully practical finite element approximations of degenerate Cahn–Hilliard systems, M2AN Math. Model. Numer. Anal. 35 (2001) 713–748.
[2] J.P. Boyd, Chebyshev and Fourier Spectral Methods, second ed., Dover, Mineola, NY, 2001.
[3] J.W. Cahn, J.E. Hilliard, Free energy of a non-uniform system I: interfacial free energy, J. Chem. Phys. 28 (1958) 258–267.
[4] L.Q. Chen, J. Shen, Application of semi-implicit Fourier-spectral method to phase field equations, Comput. Phys. Comm. 108 (1998) 147–158.
[5] M. Cheng, J.A. Warren, An efficient algorithm for solving the phase field crystal model, J. Comput. Phys. 227 (2008) 6241–6248.
[6] B. Coasta, W.-S. Don, D. Gottlieb, R. Sendersky, Two-dimensional multi-domain hybrid spectral-WENO methods for conservation laws, Commun. Comput. Phys. 1 (2006) 550–577.
[7] M.I.M. Copetti, C.M. Elliot, Kinetics of phase decomposition processes: numerical solutions to Cahn–Hilliard equation, Mater. Sci. Technol. 6 (1990) 273–283.
[8] C.M. Elliot, D.A. French, Numerical studies of the Cahn–Hilliard equation for phase separation, IMA J. Appl. Math. 38 (1987) 97–128.
[9] C.M. Elliot, D.A. French, A nonconforming finite element method for the two dimensional Cahn–Hilliard equation, SIAM J. Numer. Anal. 26 (1989) 884–903.
[10] C.M. Elliot, D.A. French, D.A. Milner, A second order splitting method for the Cahn–Hilliard equation, Numer. Math. 54 (1989) 575–590.
[11] C.M. Elliot, S. Larsson, Error estimates with smooth and nonsmooth data for a finite element method for the Cahn–Hilliard equation for phase separation, Math. Comp. 58 (1992) 603–630.
[12] D.J. Eyre, in: J.W. Bullard et al. (Eds.), Computational and Mathematical Models of Microstructural Evolution, Materials Research Society, Warrendale, PA, 1998, pp. 39–46.
[13] D.J. Eyre. <http://www.math.utah.edu/eyre/research/methods/stable.ps>.
[14] X.B. Feng, A. Prohl, Error analysis of a mixed finite element method for the Cahn–Hilliard equation, Numer. Math. 99 (2004) 47–84.
[15] D. Furihata, A stable and conservative finite difference scheme for the Cahn–Hilliard equation, Numer. Math. 87 (2001) 675–699.
[16] M.E. Gurtin, On the two-phase Stephan problem with interfacial energy and entropy, Acta Rat. Mech. Anal. 96 (1988) 199–243.
[17] L.-P. He, D.-K. Mao, B.-Y. Guo, Prediction–correction Legendre spectral scheme for incompressible fluid flow, M2AN Math. Model. Numer. Anal. 33 (1999) 113–120.
[18] Y.N. He, Y.X. Liu, Tao Tang, On large time-stepping methods for the Cahn–Hilliard equation, Appl. Numer. Math. 57 (2007) 616–628.
[19] Y.N. He, Y.X. Liu, Stability and convergence of the spectral Galerkin method for the Cahn–Hilliard equation, Numer. Meth. PDEs 24 (2008) 1485–1500.
[20] E.V.L. Mello, O.T.S. Filho, Numerical study of the Cahn–Hilliard equation in one, two and three dimensions, Phys. A 347 (2005) 429–443.
[21] R.L. Pego, Front migration in the nonlinear Cahn–Hilliard equation, Proc. Roy. Soc. London A 422 (1989) 261–278.
[22] Z.Z. Sun, A second-order accurate linearized difference scheme for the two-dimensional Cahn–Hilliard equation, Math. Comp. 64 (1995) 1463–1471.
[23] B.P. Vollmayr-Lee, A.D. Rutenberg, Fast and accurate coarsening simulation with an unconditionally stable time step, Phys. Rev. E 68 (0066703) (2003) 13.
[24] Y. Wang, L.-Q. Chen, A.G. Khachaturyan, Kinetics of strain-induced morphological transformation in cubic alloys with a miscibility gap, Acta Metall. Mater. 41 (1993) 279–296.
[25] D. Xiu, J. Shen, An efficient spectral method for acoustic scattering from rough surfaces, Commun. Comput. Phys. 1 (2007) 54–72.
[26] C. Xu, T. Tang, Stability analysis of large time-stepping methods for epitaxial growth models, SIAM J. Numer. Anal. 44 (2006) 1759–1779.
[27] J. Zhu, L.-Q. Chen, J. Shen, V. Tikare, Coarsening kinetics from a variable-mobility Cahn–Hilliard equation: application of a semi-implicit Fourier spectral method, Phys. Rev. E 60 (1999) 3564–3572.